Kinetics and Catalysis, Vol. 43, No. 6, 2002, pp. 830–837. Translated from Kinetika i Kataliz, Vol. 43, No. 6, 2002, pp. 893–901.

Copper Reinforced Catalysts on a Heat-Exchange Surface for Nitrobenzene Hydrogenation to Aniline

M. M. Danilova, N. A. Kuzin, V. A. Kirillov, E. A. Panchenko, V. D. Meshcheryakov, E. M. Moroz, and N. A. Rudina

Boreskov Institute of Catalysis, Siberian Division, Russian Academy of Sciences, Novosibirsk, 630090 Russia

Received December 28, 2001

Abstract—The methods of X-ray diffraction, mercury porosimetry, and electron microscopy are used to study the texture and phase composition of nickel–aluminum supports obtained by the sintering of nickel and aluminum powders reinforced by a stainless steel grid and distributed over a heat-exchange surface, as well as copper catalysts for nitrobenzene hydrogenation to aniline supported on these materials. The catalysts prepared using this procedure are active in this reaction and make it possible to carry it out without substantial overheatings of the surface.

INTRODUCTION

One of the problems relevant to the catalysts of exothermic reactions is the maintenance of the desired temperature regime and the prevention of overheatings resulting in catalyst sintering and deactivation. This problem cannot be solved using traditional catalysts in the form of granules, rings, and powders. One of the methods for solving this problem is the use of catalytic heat-exchange tubes, which combine the catalytic and heat-exchange surface and provide intensive heat removal [1–4].

In this study, we applied a catalytic metallic heat-exchange tube to the highly exothermic reaction of nitrobenzene hydrogenation to aniline. On the outer surface of the tube, a reinforced copper catalyst supported on nickel–aluminum-covered silica was distributed. The regularities of the formation of the nickel–aluminum support reinforced by a steel grid and distributed over the heat-exchange surface are considered in more detail than in [2]. The catalytic properties of the catalyst are tested in the reaction of gas-phase nitrobenzene hydrogenation.

EXPERIMENTAL

Metallic supports were obtained by sintering a mixture of metallic powders of nickel (PNE-1) and aluminum (PA-4). According to electron microscopic data, the predominant size of the aluminum particles in the powder was 5–15 μm, and that of nickel was 10–25 μm. The preparation procedure for reinforced supports distributed on a heat-exchange tube was described earlier in [2, 5]. Tubes were heated in a flow of argon at 800°C. Copper and the additives of chromium oxide and barium nitrate were supported by the impregnation of the support with a solution of copper, chromium, and barium nitrates. The samples were dried at 120°C, and the nitrates were decomposed in a flow of nitrogen at 250°C and reduced in a nitrogen–hydrogen mixture (10–15 vol % H_2) at 270°C. The concentration of copper in the samples was determined by X-ray fluorescent analysis using a VRA-20 analyzer, the chromium content was determined using atomic absorption spectroscopy, and that of barium was determined by the atomic emission method.[1] The specific surface area of the supports and the total surface area of the catalysts were determined by the express BET method from the thermal desorption of argon. The total pore volume and the distribution of pores over radii were determined using mercury porosimetry. For the detailed study of the pore structure, nitrogen adsorption at 77 K using a precision ASAP-2400 Micrometrics instrument was applied. The size and shape of particles were determined by scanning and transmission electron microscopy (PEN-100U and JEM-100CX instruments). X-ray analyses were carried out using an HZG-4 instrument (with monochromatized CuK_α irradiation).

The activity of the catalytic tubes was estimated from the nitrobenzene conversion determined in a flow-type reactor at atmospheric pressure. Temperature was varied in the range 150–180°C. The nitrobenzene : hydrogen ratio ranged from 1 : 3.5 to 1 : 9. Nitrobenzene was supplied with a displacement method. The amount of nitrobenzene supplied through a capillary was determined using a calibrated gauge. A quartz tubular evaporator was equipped with an electric heating element. A mixture of nitrobenzene and hydrogen vapors were supplied from the evaporator into a stainless steel reactor with a diameter of 8 mm. The reinforced catalyst was distributed over the outer surface of

[1] Characteristics of supports and catalysts with the exception of the catalytic activity refer to the porous layer separated from the reinforcing grid.

0023-1584/02/4306-0830$27.00 © 2002 MAIK “Nauka / Interperiodica”

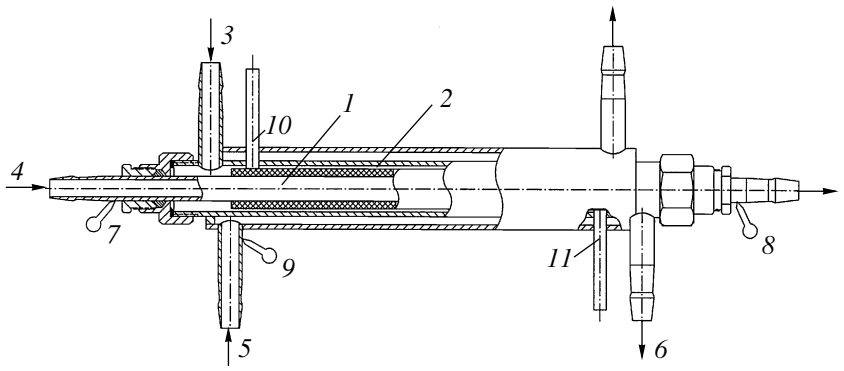

Fig. 1. Schematic of the reactor: (*1*) heat-exchange tube; (*2*) reinforced catalyst; (*3*) inlet for the reaction mixture; (*4*) inlet for the heat-carrier liquid to the heat-exchange tube; (*5*) inlet for the heat-carrier liquid to the jacket; (*6*) outlet for the products; (*7*, *8*) thermocouples in the heat-exchange tube; (*9*) thermocouple at the inlet of the reactor jacket; and (*10*, *11*) thermocouples mounted on the catalyst surface.

the reactor. The length of the catalyst coating was 15.1 cm. The diameter (together with the heat-exchange tube) was 13 mm. The catalyst volume was 12.5 cm^3. Catalysts were activated before each run by heating in a flow of hydrogen at 160°C for 1 h.

Nitrobenzene used in the reaction was distilled and purified from traces of sulfur-containing compounds using a nickel oxide–chromium catalyst. Reaction products were analyzed by GLC using an LKhM-8MD chromatograph equipped with a thermal conductivity detector. A column was graphitized with thermal soot modified by 1-nitroanilinoantraquinone. For a number of samples, the products were analyzed by chromatography coupled with mass spectrometry using a Saturn 2000GC/MS instrument with a CP 5860 capillary column.

RESULTS AND DISCUSSION

1. The Textures and Phase Compositions of Supports and Catalysts

The results of X-ray phase analysis of nickel–aluminum supports show that, with an increase in the concentration of aluminum from 10 to 30 wt %, the phase composition of supports changes (Table 1).

With an increase in the concentration of aluminum from 10 to 20 wt %, the nickel phase disappears and the amount of the $Al_{1.1}Ni_{0.9}$ phase increases. With an increase in the concentration of aluminum to 30 wt %, the phases of $Al_{1.1}Ni_{0.9}$ and Al_3Ni appear. The characteristics of the pore structure of supports are presented in Table 2 and Fig. 2. It was found that, with an increase in the concentration of aluminum from 10 to 30 wt %, the value of the specific surface area does not change substantially and remains 0.2–0.8 m^2/g; the total pore volume is also about the same and lower than 0.22 cm^3/g. Supports have a large-pore structure according to mercury porosimetry. Most of the pore volume falls to the share of pores with radii ranging from 7 to 30 μm for support I, from 10 to 35 μm for support II, and from 15 to 40 μm for support III. The large-pore character of supports is confirmed by scanning tunneling microscopic data (Fig. 3). Figure 3a shows the microscopic pattern of support I. It is seen that this material consists of roundish conglomerations with a size of 12–30 μm formed by merging the particles with a size of 3–10 μm. Interstices between conglomerations form large pores with an average radius of 10–30 μm.

For comparison, Fig. 3d shows the microscopic pattern of the initial nickel powder. It is seen that it consists of roundish aggregates with a size of 10–25 μm composed of closely packed primary particles with a size of 3–8 μm. There are aggregates of two morphological types: aggregates consisting of smooth roundish particles with a size of 5–8 μm and smaller aggregates with a size of 3–4 μm with a rough surface, which is probably due to the formation of an oxide film. Comparison of microscopic patterns of support I and the initial nickel show that sample I preserves the corpuscular pore structure and structural elements of the initial powder.

In contrast to support I, samples II and III are bodies that experienced more pronounced sintering (Figs. 3b and 3c): conglomerations forming the metallic support merge and form a body with a spongy pore structure

Table 1. Results of X-ray phase analysis of nickel–aluminum supports

Support	Composition of porous metallic support, wt %		Phase
	Ni	Al	
I	90	10	$AlNi_3$; $Al_{1.1}Ni_{0.9}$; Ni
II	80	20	$Al_{1.1}Ni_{0.9}$; $AlNi_3$
III	70	30	$Al_{1.1}Ni_{0.9}$; Al_3Ni

Table 2. Characteristics of nickel–aluminum supports and supported copper catalysts

Characteristics of the initial support					Supports with SiO_2		Characteristics of supported copper catalysts							
support	composition, wt %		V_Σ, cm^3/g	S_{sp}, m^2/g	V_Σ, cm^3/g	S_{sp}, m^2/g	catalyst	Cu, wt %	Cr_2O_3, wt %	$Ba(NO_3)_2$, wt %	V_Σ, cm^3/g	S_{sp}, m^2/g	d_{Cu}, Å	
	Ni	Al											XRD	TEM
I	90	10	0.18	0.8	0.15	13	**1**	10.7	0.27	0.11	0.15	27	230	100–200
							2	19.8	0.59	0.23	0.16	27	230	100–200
II	80	20	0.11	0.2	0.08	15	**3**	9.5	0.24	0.10	0.15	17	340	100–300
							4	17.8	0.50	0.20	0.09	11	370	150–300
III	70	30	0.22	0.2	0.21	8	**5**	16.2	0.40	0.15	0.07	18	220	80–200
							6	21.7	0.70	0.26	0.18	11	330	100–200

and the average pore radius increases. The reason for the fact that sample sintering becomes more intense with an increase in the fraction of aluminum is that the sintering of the nickel–aluminum system occurs in the presence of the liquid phase consisting of the aluminum melt (the melting point of Al is 660°C). According to [6, 7], the aluminum melt rapidly spread over the nickel particles. This leads to a drastic increase in the surface area for the interaction of components and to the acceleration of intermetallic compound formation. Therefore, the temperature drastically increases (the heats of formation ($-\Delta H$) of solid chemical compounds of nickel and aluminum $NiAl_3$, NiAl, and Ni_3Al are 38.0, 34.0, and 37.6 kcal/mol, respectively [8]). The formation of intermetallic compounds at the instant when the liquid and solid phases are in a contact occurs via the unilateral diffusion of aluminum atoms from the melt to the nickel particles. This results in an increase in the volume of solid particles and the formation of pores at the places of aluminum particles. According to the conception of sintering in the presence of a liquid phase [9, 10], capillary forces may cause restructuring: rearrangement and compacting of primary particles and their aggregates, as well as their merging near the zones of contacts. As this takes place, the density of regions with more dense initial packing increases and the density of more rough surfaces decreases. With an increase in the concentration of easily melted aluminum (above 10 wt %), the support materials under consideration are restructured: primary particles and their aggregates disappear, the structure becomes spongelike, and the average pore radius increases.

Table 3. Elementary cell parameters of supported copper

Support	Support composition, %		Catalyst*	Elementary cell parameter Cu, Å
	Ni	Al		
I	90	10	**1**	3.591
			2	3.592
II	80	20	**3**	3.618
			4	3.616
III	70	30	**5**	3.616
			6	3.616

* Catalyst numbering is the same as in Table 2.

The metallic supports obtained are characterized by high metallic strength and a high strength of coherence with the metallic grid, possibly due to the diffusion of aluminum atoms from the melt to the subsurface layer of stainless steel and the formation of intermetallic compounds. In some cases, the reinforcing grid in the samples containing 30 wt % aluminum are crippled after sintering probably because of a decrease in the linear expansion factor of the intermetallic compounds formed from aluminum and the grid iron.

To increase the surface area and dispersity of the supported copper, metallic samples were supported on silica in an amount of ~5 wt % by its impregnation with a sol. Silica was chosen as an additional support based on the literature data [11], according to which copper catalysts are very stable and active on this support. The specific surface area of support in the case of supporting SiO_2 increases to ~15–18 m^2/g (Table 2), but the total pore volume somewhat decreases (Fig. 2). According to scanning electron microscopic studies, silica is a glassy support with some fissures (Fig. 4a). According to transmission electron microscopic (TEM) data, this support is porous and consists of glob-

ules with a size ~130 Å. These globules are rather closely packed: the interstices are smaller than the species (Fig. 4b). For a more detailed study of the pore structure of SiO_2, we used the method of low-temperature nitrogen adsorption. It was shown that the support has a uniform mesoporous structure with a preferred pore radius of 3–4 nm (Fig. 5).

To determine the nature of the supported copper distribution, the catalysts were studied by TEM, which showed the presence of copper particles with a size of 100–300 Å. No noticeable change in the copper particle size was detected with an increase in the concentration of copper from 10 to 20 wt % or with an increase in the fraction of aluminum in the support (Table 2). According to the results of X-ray determination of particle sizes from the broadening of X-ray signals for the catalysts containing ~10 wt % Cu, the average copper particle size is ~200–300 Å and insignificantly changes with an increase in the concentration of copper (Table 2).

Table 3 presents the X-ray results of elementary cell parameter (ECP) measurements for crystalline copper in supported catalysts. They suggest that the values of EXP depend on the support composition. For pure copper, the elementary cell parameter is 3.607 Å. In the catalysts based on support I, it decreases to 3.591–3.592 Å. In the samples on supports II and III, the elementary cell parameter is 3.616–3.618 Å. Because the elementary cell parameter of nickel (a_{Ni} = 3.5238 Å) is lower that of copper and because the parameter of aluminum is higher than that of copper (a_{Al} = 4.0496 Å), the parameter obtained in our measurements (which is lower than for pure copper) suggests that the particles of microcrystalline copper–nickel alloy are formed in catalysts **1** and **2**. The modification of copper by nickel is probably due to the corrosion of the nickel–aluminum support during impregnation with the solution of the salts of the active component (pH of the impregnation solution is 0.8) accompanied by the extraction of nickel cations into the solution and the formation of microcrystalline alloy particles.

In catalysts **3**–**6** on supports with a high concentration of aluminum (20–30 wt %), ECP is high. Therefore, supported copper interacts with aluminum in these catalysts to form microcrystalline Cu–Al alloy particles. We assume that the diffusion of aluminum atoms from the support to copper crystals occurs in the course of active component reduction.

Thus, based on the results of X-ray study, we conclude that the active component consist of the particles of microcrystalline Cu–Ni alloy in the case of support I, and it is microcrystalline Cu–Al alloy in the case of supports II and III.

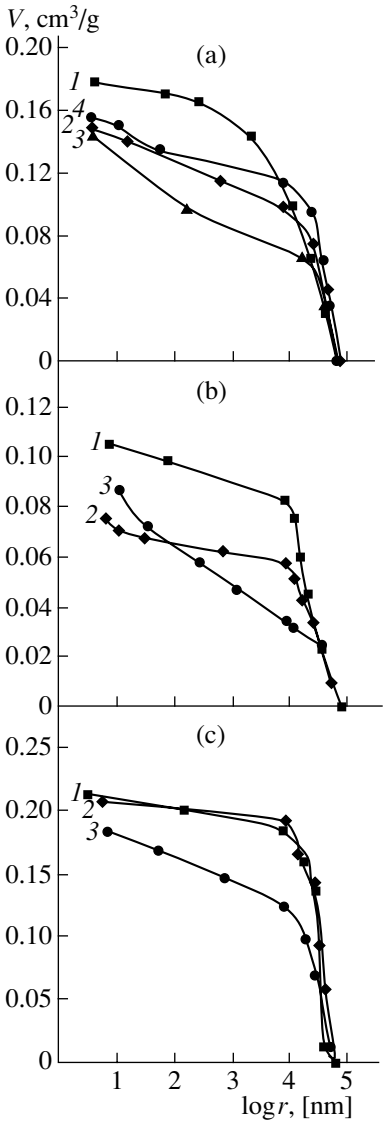

Fig. 2. Distribution of the pore volume over radii: (a) (*1*) support I, (*2*) support I with SiO_2, (*3*) catalyst **1**, (*4*) catalyst **2**; (b) (*1*) support II, (*2*) support II with SiO_2, (*3*) catalyst **4**; and (c) (*1*) support III, (*2*) support III with SiO_2, (*3*) catalyst **5**.

2. Catalytic Activity of Catalysts Distributed over Heat-Exchange Tubes

Catalytic tubes were tested in the reaction of gas-phase nitrobenzene hydrogenation.

To evaluate the possibility of nitrobenzene hydrogenation on the porous metallic support, tube 1 that did not contain copper was tested. This run was carried out at 170°C. The conversion was lower than 1% and thus was not taken into account in hydrogenation experiments.

Figure 6 shows the dependence of nitrobenzene conversion on the reaction time. It is seen that the conversion of nitrobenzene after activation on catalysts **1** and **2** immediately reaches the maximal value, whereas

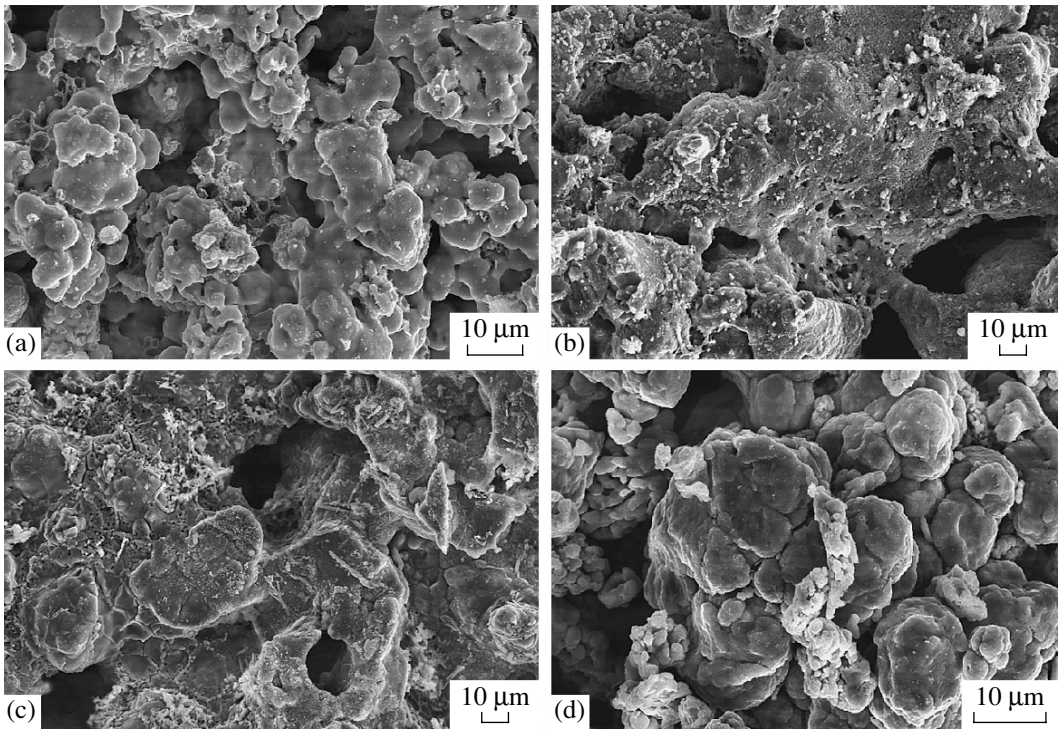

Fig. 3. Electron microscopic images of (a) support I, (b) II, (c) III, and (d) of nickel powder.

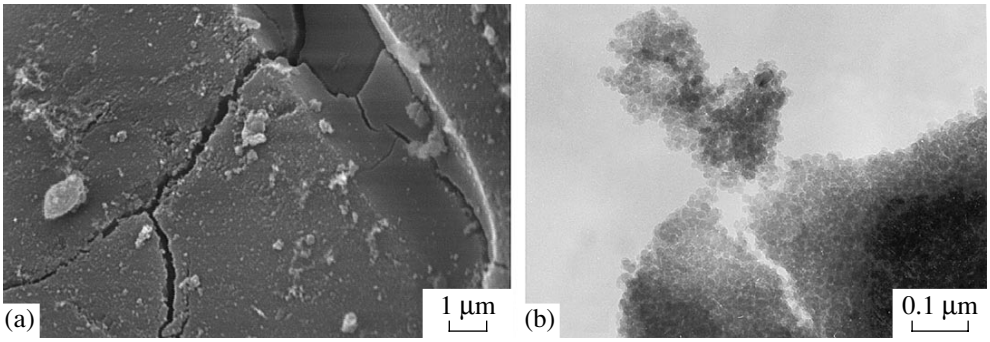

Fig. 4. Electron microscopic images of support II with SiO_2: (a) according to electron microscopic data and (b) TEM.

it reaches the maximal value under the conditions of the reaction on catalysts **3**–**6**. The apparent change in the conversion can be explained by the formation of the inactive oxide film on the catalyst surface, which contacts air: copper and nickel oxides on catalysts **1** and **2** and copper and aluminum oxides on catalysts **3**–**6**. On samples **1** and **2**, the oxide film is probably readily reduced during activation and the conversion is maximal. On catalysts **3**–**6** under the conditions of activation, the copper oxide is not reduced completely because of the interaction with poorly reducible aluminum oxide (aluminum has the highest heat of oxide formation of all the considered metals [12]). Under reaction conditions, the oxide film is reduced and the activity increases. The affect of poorly reducible aluminum oxide on the activation of supported nickel catalyst was found in [13]: an increase in the temperature of alumina-supported nickel catalyst activation compared to nickel black was observed.

Figure 7 shows data on the effect of nitrobenzene space velocity on its conversion over copper catalysts at a nitrobenzene : hydrogen ratio of 1 : 9. Comparison of the results obtained shows that the conversion of nitrobenzene increases with an increase in the concentration of supported copper from 10 to 20 wt %. This is associated with an increase in the surface area of copper per 1 g of the catalyst (Table 2). The activity of copper samples changes depending on the composition of the nickel–aluminum support. The highest conversion is observed for the catalysts on support I with a small fraction of nickel. We assume that the main reason for

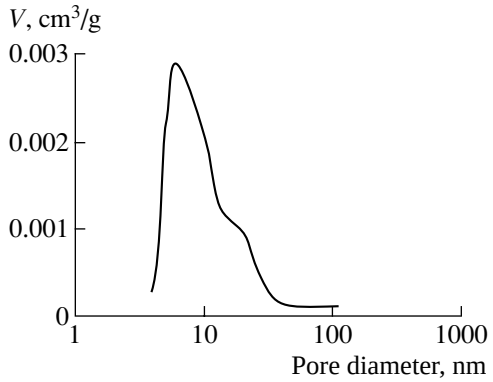

Fig. 5. Distribution of pores over radii. Support II with SiO_2. The scale along the *x* axis is logarithmic.

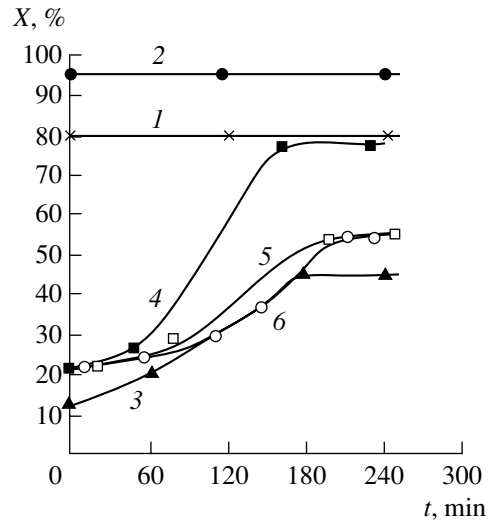

Fig. 6. Changes in the nitrobenzene conversion in the initial period of the reaction on the catalyst (*1*) **1**, (*2*) **2**, (*3*) **3**, (*4*) **4**, (*5*) **5**, and (*6*) **6**.

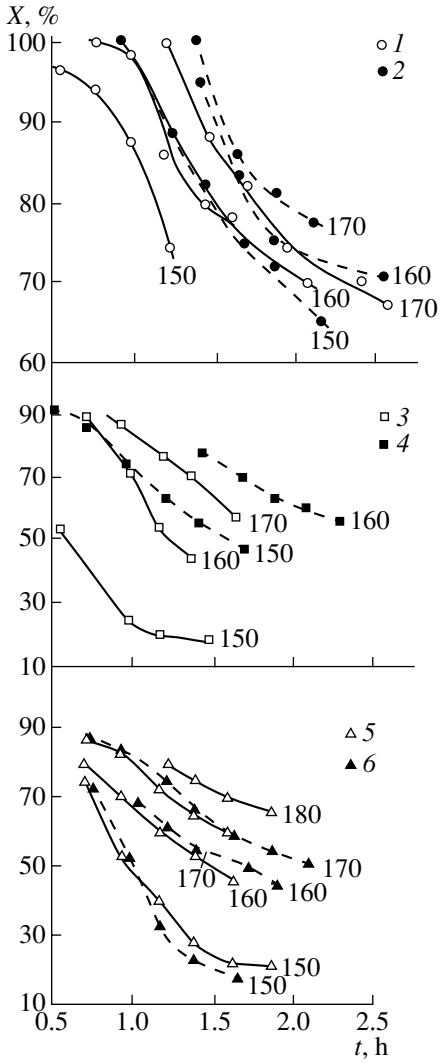

Fig. 7. Effect of the space velocity based on nitrobenzene on its conversion on catalyst: (*1*) **1**, (*2*) **2**, (*3*) **3**, (*4*) **4**, (*5*) **5**, and (*6*) **6**. Numbers are temperatures in °C.

the increase in the activity of catalysts on support I is the modification of copper by nickel with the formation of microcrystalline Cu–Ni alloy particles. An increase in the copper activity upon alloying with nickel has also been reported in the literature [14–16]. Catalysts on supports with a greater fraction of aluminum are characterized by a lower conversion. This is probably due to the interaction between copper and aluminum.

Figure 8 summarizes the results of stability tests of catalytic tubes with catalysts **1** and **6**. A decrease in the activity of sample **1** for 3000 min of time-on-stream was 28%, and that for catalyst **6** for 1500 min was 19%. Comparison of the decrease in conversion observed in this work and in [11] for copper oxide–chromium catalysts promoted with barium (0.5–0.8 mm) shows that the decrease in the activity is lower for reinforced copper catalysts probably because local overheatings are eliminated.

To restore the activity, sample **1** was subjected to oxidative–reductive treatment consisting in heating at 250°C in a flow of air for 2 h and further reduction in a nitrogen–hydrogen mixture at 270°C for 1 h. After such treatment, the initial catalyst activity was restored (the space velocity based on nitrobenzene was 1.46 h^{-1}):

Conversion, %		
initial	after 3000 min	after oxidative–reductive treatment
80.0	57.5	80.0

According to published data [1, 11, 17, 18], as well as proceeding from the fact that the catalyst activity is restored after oxidative–reductive treatment, we conclude that the decrease in the conversion observed after a long time-on-stream is due to coke formation and active site blocking.

Table 4. Temperature difference between the surface layer and the heat-carrier liquid in the heat-exchange tube ($C_6H_5NO_2 : H_2 = 1 : 9$)

Catalyst **1**

Heat-carrier temperature, °C	Space velocity based on nitrobenzene, h^{-1}						
	0.53	0.75	0.99	1.17	1.38	1.62	1.90
	Δt, °C						
150	1	1	1.5	3	–	–	–
160	2	3	3	3	4	4	–
170	–	–	–	4	4.5	5	5

Catalyst **2**

Heat-carrier temperature, °C	Space velocity based on nitrobenzene, h^{-1}						
	0.93	1.21	1.38	1.66	1.86	2.10	2.55
	Δt, °C						
150	7	8	9	13	13	13	–
160	8	–	9	10	11	10	14
170	–	–	10	10	13	14	14

Catalyst **3**

Heat-carrier temperature, °C	Space velocity based on nitrobenzene, h^{-1}				
	0.57	0.99	1.17	1.38	1.64
	Δt, °C				
150	0	2	–	1.5	–
160	2	–	–	1	1
170	–	0	0	–	1.5

Catalyst **4**

Heat-carrier temperature, °C	Space velocity based on nitrobenzene, h^{-1}						
	0.53	0.73	0.99	1.21	1.43	1.70	1.86
	Δt, °C						
150	1.5	2	1.5	2.5	2	2.5	–
160	–	4	4	4.5	3	2.5	–
170	–	–	–	4	–	3	4

Catalyst **5**

Heat-carrier temperature, °C	Space velocity based on nitrobenzene, h^{-1}					
	0.70	0.99	1.17	1.38	1.68	1.86
	Δt, °C					
150	2	3	2	2	2	3
160	1	4	5	–	–	–
170	4.5	5.5	6	–	–	–
180	–	–	6	6	–	–

Catalyst **6**

Heat-carrier temperature, °C	Space velocity based on nitrobenzene, h^{-1}					
	0.75	0.99	1.17	1.38	1.66	1.86
	Δt, °C					
150	4	5	4	3	4	–
160	3	3	4	5	5	–
170	5	5	5	5	6	6

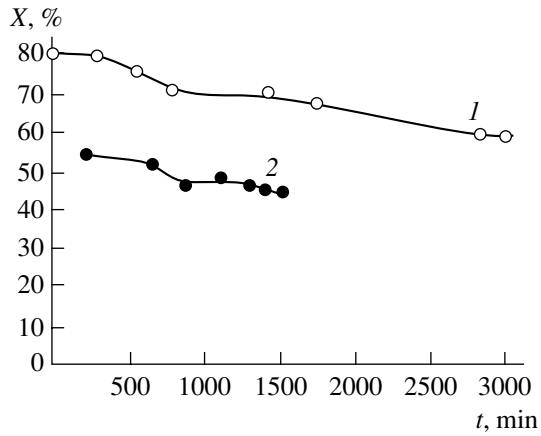

Fig. 8. Effect of the time-on-stream on the conversion of nitrobenzene. T = 160°C, the space velocity based on nitrobenzene is 1.46 h^{-1}, and the nitrobenzene : H_2 ratio is 1 : 9. Catalysts: (*1*) **1** and (*2*) **6**.

For a number of samples we determined the compositions of products using chromatography coupled with mass spectrometry. On catalyst **1**, the fraction of aniline in the products is 85–90%. The by-products are dicyclohexylamine, phenylcyclohexylamine, cyclohexanol, and benzene. With an increase in the time-on-stream, the fraction of by-products decreases, whereas it increases with an increase in the reaction temperature. On samples **3**, **4**, and **6**, the fraction of aniline in the products is 96–98%, and some unidentified compound is seen as a by-product.

In the experiments, we controlled the temperature of the reinforced catalyst using thermocouples mounted on its surface. The results of these measurements showed that the surface temperature of **3** virtually coincides with the temperature of liquid circulating inside the heat-exchange tube at all studied space velocities based on nitrobenzene. For catalysts **1**, **4**, **5**, and **6**, the difference is 2–5°C. For the most active sample **2**, the difference becomes 7–14°C when the space velocity based on nitrobenzene increase (Table 4). Experiments were carried out at a nitrobenzene : hydrogen ratio of 1 : 3.5 for catalyst **3** (Table 5). It is seen that, when the nitrobenzene : hydrogen ratio is close to the stoichiometric one, the surface temperature differs insignificantly from the temperature of the heat-carrier liquid.

Table 5. Temperature difference between the surface layer and the heat-carrier liquid in the heat-exchange tube ($C_6H_5NO_2$: H_2 = 1 : 3.5)

Catalyst **3**			
Heat-carrier temperature, °C	Space velocity based on nitrobenzene, h^{-1}		
	1.66	1.86	2.11
	Δt, °C		
180	3	3	3.5

CONCLUSION

Thus, our study showed that, when a catalytic heat-exchange tube with a reinforced copper catalyst distributed over its outer surface is used, it is possible to carry out the highly exothermic reaction of nitrobenzene hydrogenation to aniline without significant surface overheatings. We studied the formation of reinforced metallic nickel–aluminum supports distributed over a heat-exchange tube and copper catalysts supported on them. Catalysts prepared according to the proposed technique are active in the hydrogenation of nitrobenzene to aniline and have a high thermal conductivity.

REFERENCES

1. Amon, B., Redlingschofer, H., Klemm, E., *et al.*, *Chem. Eng. Proc.*, 1999, vol. 38, p. 395.
2. Danilova, M.M., Kuzin, N.A., Kirillov, V.A., *et al.*, *React. Kinet. Catal. Lett.*, 1999, vol. 69, no. 2, p. 317.
3. RF Patent 2139135, 1999.
4. Murata, K., Vumamoto, K., and Kameyama, H., *Int. J. Hydrogen Energy*, 1986, vol. 21, no. 6, p. 301.
5. RF Patent 2062402, 1996.
6. Naiborodenko, Yu.S. and Itin, V.I., *Fiz. Goreniya Vzryva*, 1975, vol. 11, no. 3, p. 343.
7. Savitskii, A.P., Martsunova, L.S., Burtsev, N.N., *et al.*, *Izv. Akad. Nauk SSSR, Met.*, 1985, no. 2, p. 191.
8. Vol, A.E., *Stroenie i svoistva dvoinykh metallicheskikh sistem* (Structure and Properties of Binary Metallic Systems), Moscow: Fizmatgiz, 1959, vol. 1, p. 400.
9. Geguzin, Ya.E., *Fizika spekaniya* (Physics of Sintering), Moscow: Nauka, 1967, p. 130.
10. Eremenko, V.N., Naidich, Yu.V., and Lavrinenko, I.A., *Spekanie v prisutstvii zhidkoi metallicheskoi fazy* (Sintering in the Presence of Liquid Metallic Phase), Kiev: Naukova Dumka, 1968.
11. Keri, H., Jharda, S., and Slicpcerich, C., *Ind. Eng. Chem.*, 1960, vol. 52, no. 5, p. 137.
12. *Spravochnik khimika: Osnovnye svoistva neorganicheskikh i organicheskikh soedinenii* (Handbook on Chemistry: Main Properties of Inorganic and Organic Compounds), Nikol'skii, B.A., Ed., Leningrad: Khimiya, 1971, vol. 1.
13. Noskova, S.P., *Cand. Sci. (Chem.) Dissertation*, Novosibirsk: Inst. of Catalysis, 1975.
14. USSR Inventor's Certificate no. 525304, *Byull. Izobret.*, 1984.
15. FRG Patent 2320658, 1972.
16. Pogorelov, V.V. and Gel'dshtein, A.I., *Kinet. Katal.*, 1976, vol. 17, no. 6, p. 1497.
17. Pasek, J. and Gerny, J., *Chem. Prumysk*, 1972, vol. 22, p. 436.
18. Petrov, L. and Kumbilieva, K., *Appl. Catal.*, 1990, vol. 59, no. 1, p. 31.